

# Hierarchical autoregressive neural networks in three-dimensional statistical system

Piotr Białas<sup>a</sup>, Vaibhav Chahar<sup>b,c</sup>, Piotr Korcyl<sup>d</sup>, Tomasz Stebel<sup>d</sup>, Mateusz Winiarski<sup>d</sup>, Dawid Zapolski<sup>a,c</sup>

<sup>a</sup>*Institute of Applied Computer Science, Jagiellonian University, ul. Łojasiewicza 11, 30-348 Kraków, Poland*

<sup>b</sup>*M. Smoluchowski Institute of Physics, Jagiellonian University, ul. Łojasiewicza 11, 30-348 Kraków, Poland*

<sup>c</sup>*Doctoral School of Exact and Natural Sciences, Jagiellonian University, ul. Łojasiewicza 11, 30-348 Kraków, Poland*

<sup>d</sup>*Institute of Theoretical Physics, Jagiellonian University, ul. Łojasiewicza 11, 30-348 Kraków, Poland*

---

## Abstract

Autoregressive Neural Networks (ANN) have been recently proposed as a mechanism to improve the efficiency of Monte Carlo algorithms for several spin systems. The idea relies on the fact that the total probability of a configuration can be factorized into conditional probabilities of each spin, which in turn can be approximated by a neural network. Once trained, the ANNs can be used to sample configurations from the approximated probability distribution and to evaluate explicitly this probability for a given configuration. It has also been observed that such conditional probabilities give access to information-theoretic observables such as mutual information or entanglement entropy. So far, these methods have been applied to two-dimensional statistical systems or one-dimensional quantum systems. In this paper, we describe a generalization of the hierarchical algorithm to three spatial dimensions and study its performance on the example of the Ising model. We discuss the efficiency of the training and also describe the scaling with the system's dimensionality by comparing results for two- and three-dimensional Ising models with the same number of spins. Finally, we provide estimates of thermodynamical observables for the three-dimensional Ising model, such as the entropy and free energy in a range of temperatures across the phase transition.

*Keywords:* Variational Autoregressive Neural Networks, Hierarchical Neural Networks, Spin Systems, three-dimensional Ising model, Markov Chain Monte Carlo

---

## 1. Introduction

The recent idea [1, 2] of employing artificial neural networks in Monte Carlo simulations has given birth to a new class of algorithms that promise to outperform traditional state-of-the-art algorithms, such as the cluster algorithm [3]. In many cases, this objective still remains a future goal because of the problematic scaling with the system size and difficulties in training the neural networks. Hence, the quest for more optimal neural network architectures, see for example [4, 5, 6]. However, several works have observed that such new algorithms can provide access to observables that are difficult to estimate or completely unavailable in traditional Markov Chain Monte Carlo. Examples of such observables include thermodynamic quantities such as the free energy, entropy [7, 8] or information-theoretic observables such as mutual information [9] and quantum entanglement entropy [10]. So far, most applications have been performed for two-dimensional statistical systems or one-dimensional quantum systems.

The hierarchical algorithm proposed in Ref. [11] uses a set of autoregressive neural networks [7] that enable the recursive fixing of all spins on a square lattice. It was devised for two-dimensional spin systems and was benchmarked in the Ising model on a square lattice. The construction relies on the Hammersley-Clifford theorem [12, 13] and the Markov field property of the Ising model, i.e. as long as the interactions are nearest-neighbor only, for any closed

---

*Email addresses:* piotr.bialas@uj.edu.pl (Piotr Białas), vaibhav.chahar@doctoral.uj.edu.pl (Vaibhav Chahar), piotr.korcyl@uj.edu.pl (Piotr Korcyl), tomasz.stebel@uj.edu.pl (Tomasz Stebel), mateusz.m.winiarski@student.uj.edu.pl (Mateusz Winiarski), dawid.zapolski@doctoral.uj.edu.pl (Dawid Zapolski)

contour the probabilities of any spin inside the contour depend conditionally on the values of spins from the boundary. However, the theorem underlying this idea is valid for systems of any number of dimensions.

The goal of this work is to provide a generalization of the hierarchical algorithm to three dimensions and to benchmark its scaling with the system size and the training efficiency. We shall also compare it with the architectures based on convolutional networks. We demonstrate the algorithm using the example of the Ising model.

We consider  $N = L^3$  spins that are located on a  $L \times L \times L$  periodic lattice. The Hamiltonian evaluated on a given configuration of spins,  $\mathbf{s} = \{s^i\}_{i=1}^N$  gives the energy:

$$H(\mathbf{s}) = -J \sum_{\langle i,j \rangle} s^i s^j, \quad (1)$$

where the sum runs over all neighboring pairs of lattice sites and  $s^i = \pm 1$ . We set the coupling constant  $J = 1$ , and hence ferromagnetic interactions are considered. Then, each configuration  $\mathbf{s}$  appears with the Boltzmann probability

$$p(\mathbf{s}) = \frac{1}{Z} \exp(-\beta H(\mathbf{s})), \quad (2)$$

where  $Z$  is the partition function  $Z = \sum_{\mathbf{s}} \exp(-\beta H(\mathbf{s}))$  and the sum is performed over all  $2^N$  configurations.

## 2. Neural samplers

### 2.1. Autoregressive networks

The basic idea of the Variational Autoregressive Networks (VAN) [7] is to represent the probability distribution of the spin configuration (2) as a product of  $N - 1$  conditional probabilities:

$$p(\mathbf{s}) = p(s^1) \prod_{i=2}^N p(s^i | s^1, \dots, s^{i-1}). \quad (3)$$

The analytic form of conditional probabilities  $p(s^i | \cdot)$  is not known, however, one can use neural networks to approximate them. We denote by  $q_\theta(s^i | \cdot)$  the neural approximation, where the subscript  $\theta$  indicates the weights of the neural networks. Then,

$$q_\theta(\mathbf{s}) = q_\theta(s^1) \prod_{i=2}^N q_\theta(s^i | s^1, \dots, s^{i-1}), \quad (4)$$

is the probability distribution of spin configurations provided by the network. There are two crucial properties of the algorithm. First, the network enables a direct sampling of the probability distribution  $q_\theta$ , which is not possible for the target distribution  $p$ . Second, network training enables  $q_\theta$  to be a good approximation of  $p$ ,  $q_\theta \approx p$ .

In the VAN algorithm [7], the generation of spin configurations is performed using a single neural network that takes as input the values of the consecutive spins and gives at the output the probabilities of the spins to have value  $+1$ . The network is evaluated  $N$  times and at  $i$ -th evaluation the (conditional) probability distribution of the  $i$ -th spin,  $q_\theta(s^i | s^1, \dots, s^{i-1})$ , is calculated based on the values of the  $i - 1$  spins fixed in the previous steps. Then, the  $i$ -th spin is fixed using its probability distribution. In principle, such an algorithm can sample any spin system in arbitrary dimensions with any type of interaction.

The architecture of the network needs to follow the functional dependencies of the conditional probabilities, namely  $i$ -th network's output must depend only on the first  $i - 1$  inputs (hence the name "autoregressive"). To realize this in practice, we rely either on dense layers where some of the weights are multiplied by 0 to "remove" unwanted connections between the neurons or on the convolutional networks with masked kernels (see Section 3.2 for more details).

The ability of the VAN algorithm to sample from the distribution  $q_\theta$ , where the probability of the spin configuration is explicitly calculated, allows for so-called reverse training using the (reverse) Kullback–Leibler (KL) divergence,

$$D_{KL}(q_\theta | p) = \sum_{\mathbf{s}} q_\theta(\mathbf{s}) \log \frac{q_\theta(\mathbf{s})}{p(\mathbf{s})} = E[\log q_\theta(\mathbf{s}) - \log p(\mathbf{s})]_{q_\theta(\mathbf{s})}. \quad (5)$$

The KL divergence measures the difference between two probability distributions  $q$  and  $p$ :  $D_{KL}(q|p) \geq 0$  and  $D_{KL}(q|p) = 0 \Leftrightarrow q = p$  (note however that in general  $D_{KL}(q|p) \neq D_{KL}(p|q)$  so  $D_{KL}$  is not a distance in the mathematical sense).

One estimates the average on the r.h.s. using some batch of  $n$  samples drawn from distribution  $q_\theta$ :

$$E[\dots]_{q_\theta} \rightarrow \frac{1}{n} \sum_{i=1}^n (\dots), \text{ where } \mathbf{s}_i \sim q_\theta. \quad (6)$$

When  $p$  is given by (2), one defines:

$$\hat{F}_q = \frac{1}{n} \sum_{i=1}^n (\log q_\theta(\mathbf{s}_i) + \beta H(\mathbf{s}_i)), \quad \mathbf{s}_i \sim q_\theta, \quad (7)$$

which is minimized during the network training. Minimizing  $\hat{F}_q$  is equivalent to minimizing (5), as they differ by the additive constant, which is an estimator of the free energy:

$$F = -\frac{1}{\beta} \log Z. \quad (8)$$

## 2.2. Neural importance sampling (NIS)

In practice, there is always some difference between  $p$  and  $q_\theta$  as the networks cannot be perfectly trained. This difference introduces a bias when the mean values of observables are calculated. In this manuscript, we shall use the so-called Neural importance sampling (NIS) [2] method to get unbiased results, that is based on the reweighting procedure<sup>1</sup>:

$$\langle O \rangle = \frac{1}{N\hat{Z}} \sum_{i=1}^N \hat{w}(\mathbf{s}_i) O(\mathbf{s}_i), \quad \mathbf{s}_i \sim q_\theta, \quad (9)$$

where the so-called importance ratios are defined as

$$\hat{w}(\mathbf{s}_i) = \frac{e^{-\beta H(\mathbf{s}_i)}}{q_\theta(\mathbf{s}_i)} \quad (10)$$

and the estimate of the partition function is given by:

$$\hat{Z} = \frac{1}{N} \sum_{i=1}^N \hat{w}(\mathbf{s}_i), \quad \mathbf{s}_i \sim q_\theta. \quad (11)$$

It is easy to see that when  $q_\theta = p$  one has  $\hat{w}(\mathbf{s}_i) = Z$  for all  $\mathbf{s}_i$  and (9) reduces to the standard average. When  $q_\theta \neq p$ , the importance weights depend on the configuration, and the reweighting (9) compensates for the deviation between those two distributions.

Two notes are in order here. First, it is crucial for the NIS method that  $q_\theta(\mathbf{s}_i)$  is known<sup>2</sup> and  $> 0$  for all generated configurations  $\mathbf{s}_i$ . Second, the definition (11) provides an unbiased estimator of the partition function  $Z$ , hence NIS gives access to any thermodynamical observable that may be obtained from  $Z$ . This is the most significant advantage of NIS compared to standard Monte Carlo algorithms, where getting  $Z$  is cumbersome.

In the context of the NIS, a natural measure of difference between  $q_\theta$  and  $p$  is the Effective Sample Size (*ESS*) [14, 15]:

$$ESS = \frac{\langle \hat{w} \rangle_{q_\theta}^2}{\langle \hat{w}^2 \rangle_{q_\theta}} \approx \frac{\left( \sum_{i=1}^N \hat{w}(\mathbf{s}_i) \right)^2}{N \sum_{i=1}^N \hat{w}^2(\mathbf{s}_i)}, \quad (12)$$

where  $\approx$  denotes the approximation of finite batch size of samples drawn from  $q_\theta$ . Values of *ESS* are in the range  $(0, 1]$  and for  $q_\theta = p$  one has  $ESS = 1$ .<sup>3</sup>

<sup>1</sup>In the alternative approach, Neural Markov Chain Monte Carlo (NMCMC) [1, 2], one uses the accept-reject step on configurations generated by the network.

<sup>2</sup>Some generative models can generate configurations but are unable to provide their probability, for instance GANs.

<sup>3</sup>Note that  $ESS = 1$  does not mean that  $q_\theta = p$  since the mode seeking may occur:  $\sup q_\theta \neq \sup p_\theta$ .

### 3. Architectures of networks

#### 3.1. Hierarchical autoregressive networks

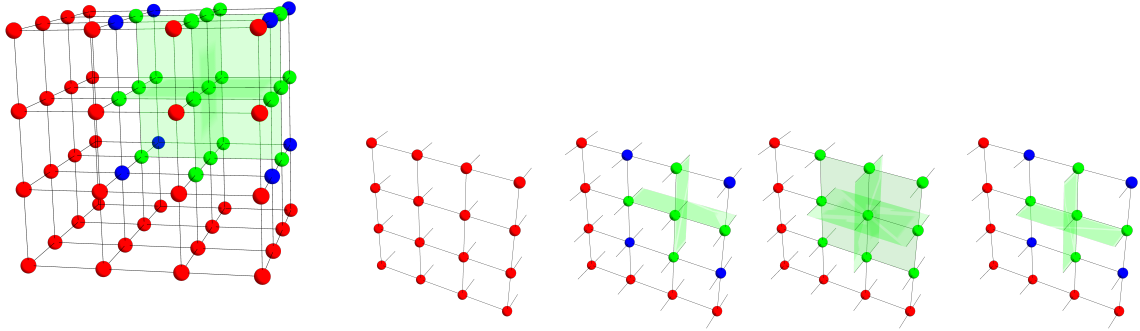


Figure 1: Example of a hierarchical partitioning in 3D for  $L = 4$ . On the first level, the red boundary  $B^{(0)}$  is generated with one neural network  $\mathcal{N}_0$ . At the second level of the hierarchy, one neural network of smaller size  $\mathcal{N}_1$  is used to consecutively fix a set of boundaries shown in green, what makes a network  $B^{(1)}$ . The remaining empty spins (marked in blue) corresponding to  $I^k \equiv B^{(2),k}$ ,  $k = 1, \dots, 8$  have all the neighbors fixed and therefore can be generated from a local Boltzmann distribution with the heatbath algorithm.

In the VAN algorithm, it is necessary to evaluate the neural network  $N$  times to fix all  $N$  spins. Since all conditional probabilities (4) are provided by a single network, this network must have  $N$  input and  $N$  output neurons. In the implementation of VAN based on dense neural networks, the number of weights of the network scales as  $\sim N^2$ . Assuming that the whole matrix multiplications are performed (which is usually true, due to the ease of implementation), the cost of generating one configuration scales as  $\sim N^3$ , which is  $\sim L^9$  for 3D systems. With a different implementation, where for the given conditional probability only the necessary weights get multiplied, this scaling in principle can be reduced to  $\sim L^6$  (for VAN) or  $\sim L^4$  (for HAN). However, the gains are not immediately obvious as they depend on the size of the problem and the capacity of the GPU. Such implementation is in progress, but its study is beyond the scope of this paper.

Following the idea of HAN in 2D, we replace a single neural network from the VAN approach by a set of smaller neural networks. In Fig. 1 we show a schematic representation of the spin system of size  $4 \times 4 \times 4$  and demonstrate its partition into recursive subsets. Periodic boundary conditions are imposed, namely, spins in the outer wall interact with the spins in the opposite wall. In the HAN algorithm, we start with the so-called boundary spins, denoted by red dots in Fig. 1 and using a standard autoregressive network we fix their values - we call this the first step of the networks' hierarchy. This neural network will form the top of the neural networks hierarchy. Thanks to periodic boundary conditions, these three walls provide the boundary that encloses the interior of the system (in Fig. 1 interior is a  $3 \times 3 \times 3$  cube of spins denoted with green and blue dots).

In the second stage of the hierarchy, the second network is used to fix the 3d cross-like structure, denoted by green dots in Fig. 1. The network takes as an input not only the values of spins denoted as green dots, but also the red ones. As the output, it provides conditional probabilities for the green spins. This dependence on the boundary spins was introduced by adding additional input to dense layers keeping the autoregressive dependence of the generated spins, see Fig. 2 in Ref. [11] for the schematic graph.

For  $L = 4$  the hierarchy ends with 8 blue spins, which are isolated (in the sense that all their neighbors' values are fixed). The isolated spin can be fixed using the heatbath algorithm, namely one explicitly calculates the probability of the spin  $s^i$  to be +1 from the expression:

$$q(s^i = +1, n(s^i)) = \left[ 1 + \exp \left( -2\beta \sum_{j \in n(s^i)} s^j \right) \right]^{-1}, \quad (13)$$

where the sum is performed over neighbors  $n(s^i)$  of the spin  $s^i$ .

This hierarchy can be straightforwardly extended to larger systems when  $L = 2^k$ ,  $k \geq 2$ . For  $L = 8$  at the first stage of the hierarchy one needs to fix spins on 3 walls, each of size  $8 \times 8$ , 169 spins in total because some spins are shared between walls. In the second stage, the 3D cross-like structure has a size of 7 spins in every dimension and divides the spins into 8 cubes each of size  $3 \times 3 \times 3$ . At this stage, we can use the same network architecture as that used in the  $4 \times 4 \times 4$  system. Note that the conditional probabilities of those spins have the same functional dependencies on the surrounding spins (according to the Hammersley-Clifford theorem). Therefore, the spins in all 8 cubes (of size  $3 \times 3 \times 3$ ) can be fixed simultaneously using only one network. In other words, at this stage of hierarchy we have only one network, that fixes the spins in all 8 cubes. The last stage of hierarchy is the isolated spins, that are fixed using the heatbath formula.

The procedure for  $L = 16, 32, \dots$  follows the same algorithm. Going from  $k$  to  $k + 1$  (where  $L = 2^k$ ), requires: i) adding (in the second stage) a new network and ii) increasing the size of the first network which fixes boundary spins (red).

The scaling with system size of the 3D hierarchical algorithm is  $\sim L^6$ : this is easy to see since the boundary and cross-like structures grow with  $L$  as a surface (not a volume), hence  $\sim L^2$ . Then, we have the scaling of the HAN 3D the same as the scaling of the VAN 2D - this is even more understandable if one notices that the architecture of the boundary network (red spins in Figure 1) is just the VAN 2D. Summarizing, in 3D, the  $\sim L^9$  scaling of the VAN is reduced to  $\sim L^6$  of the HAN.

We used the same hyperparameters for the VAN and HAN networks: we always use dense networks with two layers, an ADAM optimizer was chosen, and the learning rate was set to 0.001.

### 3.2. PixelCNN VAN and Gated PixelCNN VAN

In this section, we discuss the convolutional neural networks (CNN) version of the VAN [7]. It is based on the PixelCNN network used to generate images [16] and we will refer to it as PixelCNN VAN. The autoregressive property is assured by using a masked kernel (a kernel with some elements multiplied by zero).

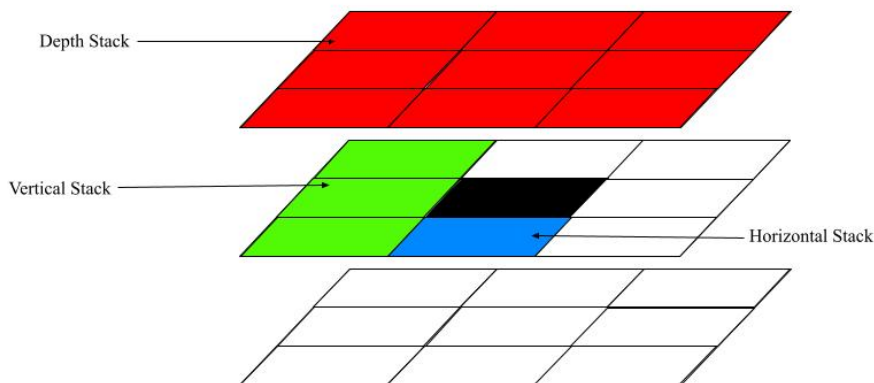


Figure 2: A 3D kernel of PixelCNN. The kernel is divided into stacks. Elements multiplied by 0 are denoted with white color.

The original PixelCNN VAN [7] was designed for 2D systems, so we upgraded the code to 3D. In Fig. 2 we show a schematic view of the masked  $3 \times 3 \times 3$  3D kernel. The red, green, and blue colors denote different parts of the kernel, called stacks. The white elements are multiplied by 0 (masked) so that the autoregressive property is preserved. The black element is either zero (which means a strictly autoregressive layer) or non-zero (weakly autoregressive layer).

In reference [16] authors propose some improvements to the PixelCNN architecture. They note that the masking pattern leads to a blind spot in the receptive field even after applying many layers. To fix this, they propose to split the kernel into vertical and horizontal stacks. When adapting this architecture to 3D we have added the third depth stack (see Fig. 2). The information from depth is flowed into both vertical and horizontal stacks and from vertical to horizontal stack using  $1 \times 1 \times 1$  convolutions (see Figure 3 left). To ensure that the model is autoregressive, the depth stack does not receive information from the vertical and horizontal stacks, and the vertical stack is blinded to information from the horizontal stack. The output of each stack is then fed into the Exponential Linear Unit (ELU)

activation function. Finally, a residual connection is added to the output of each stack, and a skip connection is drawn from the output of the horizontal stack. We follow [16] also in the use of the *gated architecture*: another mirror CNN produces a signal (number between zero and one) that is used to *gate* the output from the first CNN by multiplying it. Authors claim that this enhances the model performance. The architecture of the gated 3D PixelCNN is shown in the right part of Fig. 3. The input is a 3D spin configuration, as for VAN/HAN architectures. The network consists of several gated layers, where the first one is strictly autoregressive (s.a.), and the rest are weakly autoregressive. The final output is the sum of all the skip connections coming from layers fed into the sigmoid function to get the conditional probabilities of the spins.

The right panel of Figure 3 shows a schematic view of a single gated layer. To ensure that the model is autoregressive, the depth stack does not receive information from the vertical and horizontal stacks, and the vertical stack is blinded to information from the horizontal stack. The output of each stack is then fed into the Exponential Linear Unit (ELU) activation function. Finally, a residual connection is added to the output of each stack, and a skip connection is drawn from the output of the horizontal stack.

For convolutional networks, one expects  $\sim L^6$  scaling with a system size: the number of convolutions needed to calculate a given conditional probability scales as  $\sim L^3$ ; the number of spins scales as  $\sim L^3$ .

We used the same hyperparameters for PixelCNN and gated PixelCNN: networks consist of 6 layers, with 18 channels and kernel  $5 \times 5 \times 5$ ; an optimizer was ADAM and the learning rate was set to 0.003.

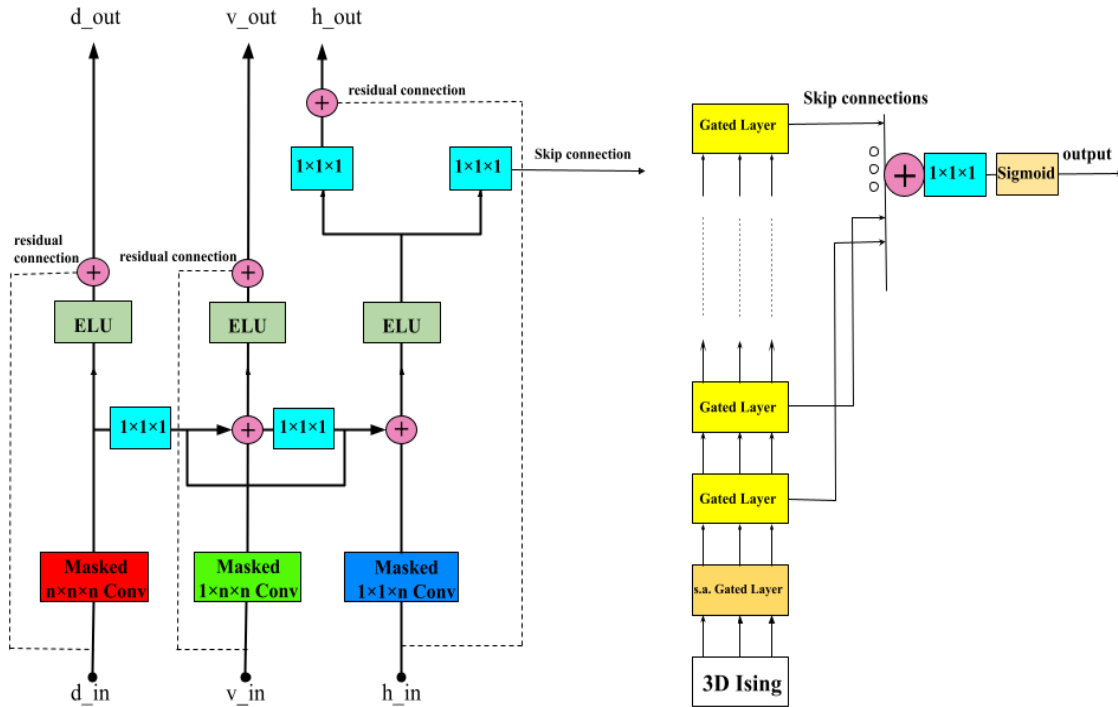


Figure 3: Left: schematic view of one gated PixelCNN layer. Right: architecture of gated PixelCNN network. See text for the description.

## 4. Numerical results

### 4.1. Timings and ESS for autoregressive architectures

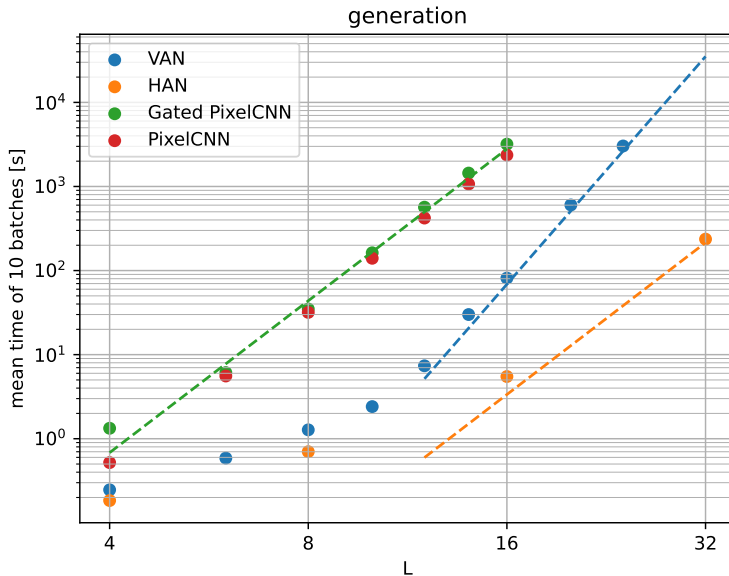


Figure 4: Mean time (in seconds) of 10 batches generation of VAN (blue circles), HAN (orange circles), PixelCNN (red circles) and Gated PixelCNN (green circles) algorithms in dependence on system linear size  $L$ . Asymptotic approximations  $\alpha L^9$  (blue dashed line),  $\beta L^6$  (orange dashed line) and  $\gamma L^6$  (green dashed line), for VAN, HAN and Gated PixelCNN accordingly, were superposed on plots. All the measurements were performed on Nvidia GeForce 4090 GPU.

We shall start by comparing different sampling algorithms when it comes to the configuration generation time<sup>4</sup>. We compare the generation time of 10 batches of 1024 configurations for the architectures described in Section 3. In Fig. 4 we show the dependence on the linear system size  $L$  on a log-log scale. First, we note that CNN-based architectures are significantly slower (an order of magnitude in the presented range of system sizes) than the VAN architecture based on dense networks. The HAN architecture is faster than VAN, as expected, and they have different scaling with system size, as we discussed in section 3.1. To better visualize the scaling of the architectures, we have added the lines in Fig. 4, which represent scaling  $L^9$  (blue line) and  $L^6$  (yellow and green line). For small system sizes, the scaling is modified by other effects (*e.g.* saving data), but for larger  $L$  we observe the expected scaling for all algorithms. Also, the timing scaling of CNN architectures follows expected  $\sim L^6$  behavior.

The final *ESS* for Gated PixelCNN and HAN are similar, reaching around 0.95 for  $L = 8$  and close to the phase transition. For the PixelCNN this value is smaller, around 0.4. Finally, the VAN reaches around 0.6. Hence, we conclude that with current architectures, dense networks are more suitable for autoregressive networks. In what follows, we focus on the HAN algorithm as the most efficient.

### 4.2. Physical observables

We shall now cross-check the results obtained using HAN for some physical observable using MCMC. For this purpose, we use an in-house implementation of the Wolff cluster algorithm [3]. It is one of the state-of-the-art algorithms used in simulations of Ising model due to a significantly reduced (compared to local-update Monte Carlo like Metropolis algorithm) problem of critical slowing down close to the phase transition. At each step one builds a cluster

<sup>4</sup>Since in autoregressive networks, numerical cost of training is dominated by the generation of the configurations, the conclusions of this analysis apply to training timings as well.

of spins (where the probability of a spin to be attached to the cluster depends on  $\beta$ ) and then the spins in the cluster are flipped.

We start with the simulation of mean absolute magnetization per spin defined as:

$$\langle |M| \rangle = \left\langle \frac{1}{N} \left| \sum_{i=1}^N s^i \right| \right\rangle_p. \quad (14)$$

In the limit of an infinite volume ( $L \rightarrow \infty$ ), this quantity is an order parameter of the system with  $\langle |M| \rangle = 0$  for  $\beta \rightarrow 0$  (disordered phase, high temperature),  $\langle |M| \rangle = 1$  for  $\beta \rightarrow \infty$  (ordered phase, low temperature) and the phase transition at  $\beta_c \approx 0.2215$ .

In Fig. 5 (left) we show  $\langle |M| \rangle$  as a function of  $\beta$  calculated for  $L = 8$  using two methods: HAN (with NIS) and Wolff algorithm. One can see very good agreement with the errors below 1‰, where the errors were obtained using the bootstrap method – see the inset which shows the difference of the two results. In the right panel of Figure 5 we show the mean energy  $\langle E \rangle$ , where a similar agreement can be observed.

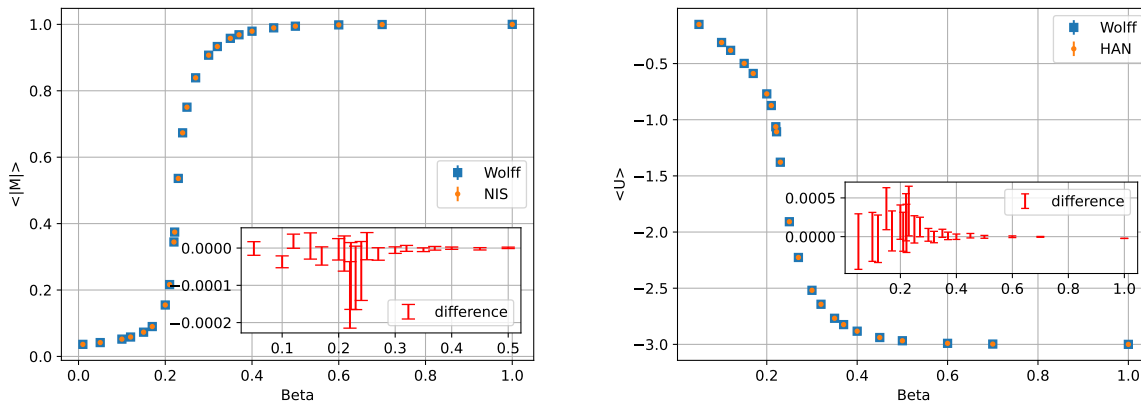


Figure 5: Comparison of the HAN (with NIS) with the Wolff algorithm for absolute magnetization per spin (left panel) and energy (right panel). Insets show difference of two results.

After cross-checking our results against the Markov chain Monte Carlo, we move to the observables that are not possible to calculate with this method. In Figure 6, we show results for the free energy per spin  $F/N$  (8) and entropy per spin:

$$S = \frac{\beta}{N} (\langle E \rangle - F), \quad (15)$$

where both quantities were calculated with the NIS method. We show results for  $L = 4$  and  $L = 8$ , demonstrating a weak dependence on the size of the system.

#### 4.3. HAN versus Wolff algorithm: timings

It is also instructive to compare the speed of our HAN 3D algorithm with that of the Wolff cluster algorithm. Here we are not aiming for a precise comparison, since we used in-house code (with some optimizations) for the Wolff algorithm. We shall make this comparison just to give the reader a rough idea of a HAN timing. The exact comparison of the algorithms is difficult, also due to their very different nature. For example, Wolff algorithm in principle is sequential; however, one can still run multiple Markov Chains simultaneously on the GPU. Both, the Wolff algorithm and HAN, were run on the same device: a high-performance Nvidia GeForce 4090 GPU.

The training of our HAN model at  $\beta = 0.264$  and  $L = 8$  took  $\sim 430$ s and reached  $ESS = 0.968$ . With this model, we generated  $5 \times 10^8$  configurations and, using NIS, calculated the relative error of the absolute magnetization equal to  $2.6 \times 10^{-6}$ . The generation of configurations took  $\sim 3400$ s. To reach the same precision using the Wolff algorithm,



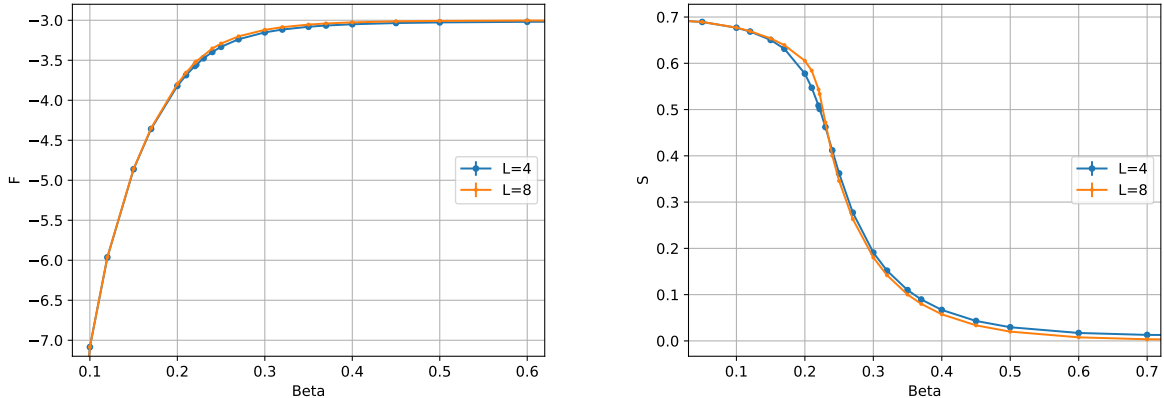


Figure 6: Free energy (left) and entropy (right) obtained using HAN (with NIS) for two system size:  $L = 4$  (blue) and  $L = 8$  (yellow).

one needs  $1.2 \times 10^9$  configurations, where the autocorrelation time was measured to be 2.6. It takes  $\sim 47$  s to generate them using 32768 parallel chains.

Summarizing this rough comparison, the same precision for the observable was obtained with the cluster algorithm  $\sim 70$  times faster than with our HAN 3D model (training and generation). It is worth noting that running the Wolff algorithm on a single CPU core is a few hundred times slower than using a GPU in our case. This is because of the small autocorrelation time, which allows for massive parallelization speed-up.

#### 4.4. Efficiency of training in 2D and 3D

Here we compare how the HAN algorithm works in 2D and 3D systems. For this purpose, we consider a 2D system  $8 \times 8$  at  $\beta = 0.38$  and a 3D system  $4 \times 4 \times 4$  at  $\beta = 0.22$ . The temperatures were chosen such that the magnetization is around 0.5 in both cases. The number of spins is the same in both systems, so the difference in training comes from the different setup of networks<sup>5</sup> and different correlations between spins in 2D and 3D.

In Figure 7, we plot the ESS as a function of training epochs for those two versions of the HAN algorithm. We used the same hyperparameters for dense networks (2 layers) and the same learning rate 0.005. For each system, we run the training 5 times (curves of the same color). One can observe that ESS grows faster for 3D HAN than in 2D. The timings are the following: 500 epochs of training the 3D HAN last around 8.4 seconds and around 10 seconds for the 2D HAN.

## 5. Summary

In this paper, we have presented the hierarchical autoregressive network (HAN) algorithm suited for 3-dimensional spin systems and compared it with three other architectures: conventional variational autoregressive networks (VAN), autoregressive convolutional networks (PixelCNN), and a gated version of autoregressive convolutional networks (gated PixelCNN). We have performed several tests concerning the efficiency of 3D algorithms using classical Ising model: i) scaling with the system size, ii) comparison with the Wolff algorithm (concerning the evaluation of physical observables as well as the timings). We have found that HAN 3D is the fastest of all the architectures tested and allows good training quality (measured  $ESS \approx 0.95$ ) in the system  $8 \times 8 \times 8$ . A rough comparison shows that for such a system, the Wolff cluster algorithm is much faster (factor  $\sim 70$ ) on the same device. On the other hand, Wolff algorithm (and any other MCMC method) does not allow for estimation of thermodynamical observables like free energy and entropy. We calculated those using HAN (combined with NIS).

<sup>5</sup>HAN 2D in  $8 \times 8$  system uses 3 networks and HAN 3D in  $4 \times 4 \times 4$  system uses 2 networks.

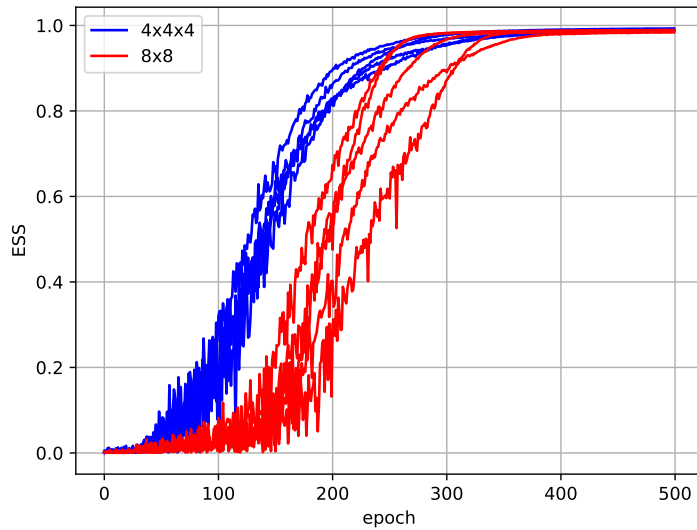


Figure 7: Comparison of the ESS growth for  $4 \times 4 \times 4$  (blue) and  $8 \times 8$  (red) systems in a corresponding critical temperature (0.22 for the 3D and 0.38 for the 2D system) with the learning rate set to 0.005 and the batch size of 8196

In our opinion, the fact that autoregressive networks can be used to calculate observables inaccessible using standard MCMC algorithms should be the main reason for the development of them. This manuscript is a step towards developing methods to calculate entropy, quantum entanglement entropy, and classical mutual information in 3D systems. Those quantities have been challenging to obtain using other methods, like tensor networks or Monte Carlo based on the Jarzynski equality [17]. The main obstacle for using NIS in 3D (and 4D) is the scalability of the neural samplers with system size. Although HAN is a good first step in this direction, much improvement is needed. Such improvement may come with new architectures developed for general-purpose Machine Learning.

## Acknowledgments

Computer time allocation ‘plnglft’ on the Athena supercomputer hosted by AGH Cyfronet in Kraków, Poland was used through the Polish PLGRID consortium. T.S. and D.Z. kindly acknowledge support of the Polish National Science Center (NCN) Grant No. 2021/43/D/ST2/03375. P.K. acknowledges support of the Polish National Science Center (NCN) grant No. 2022/46/E/ST2/00346. D.Z. acknowledges the support of the Research Support Module under the program Excellence Initiative - Research University at the Jagiellonian University. This research was partially funded by the Priority Research Area Digiworld under the program Excellence Initiative – Research University at the Jagiellonian University in Kraków.

## References

- [1] M. S. Albergo, G. Kanwar, P. E. Shanahan, Flow-based generative models for markov chain monte carlo in lattice field theory, *Phys. Rev. D* 100 (2019) 034515. URL: <https://link.aps.org/doi/10.1103/PhysRevD.100.034515>. doi:10.1103/PhysRevD.100.034515.
- [2] K. A. Nicoli, S. Nakajima, N. Strodthoff, W. Samek, K.-R. Müller, P. Kessel, Asymptotically unbiased estimation of physical observables with neural samplers, *Phys. Rev. E* 101 (2020) 023304. [arXiv:1910.13496](https://arxiv.org/abs/1910.13496).
- [3] U. Wolff, Comparison between cluster monte carlo algorithms in the ising model, *Physics Letters B* 228 (1989) 379–382. URL: <https://www.sciencedirect.com/science/article/pii/0370269389915633>. doi:[https://doi.org/10.1016/0370-2693\(89\)91563-3](https://doi.org/10.1016/0370-2693(89)91563-3).
- [4] I. Biazzo, The autoregressive neural network architecture of the boltzmann distribution of pairwise interacting spins systems, *Communications Physics* 6 (2023). URL: <http://dx.doi.org/10.1038/s42005-023-01416-5>. doi:10.1038/s42005-023-01416-5.
- [5] I. Biazzo, D. Wu, G. Carleo, Sparse autoregressive neural networks for classical spin systems, 2024. [arXiv:2402.16579](https://arxiv.org/abs/2402.16579).
- [6] A. Singha, E. Cellini, K. A. Nicoli, K. Jansen, S. Kühn, S. Nakajima, Multilevel generative samplers for investigating critical phenomena, in: *The Thirteenth International Conference on Learning Representations*, 2025. URL: <https://openreview.net/forum?id=YcUV5apdlq>.

- [7] D. Wu, L. Wang, P. Zhang, Solving Statistical Mechanics Using Variational Autoregressive Networks, *Phys. Rev. Lett.* 122 (2019) 080602. doi:10.1103/PhysRevLett.122.080602. [arXiv:1809.10606](#).
- [8] K. A. Nicoli, C. J. Anders, L. Funcke, T. Hartung, K. Jansen, P. Kessel, S. Nakajima, P. Stornati, Estimation of Thermodynamic Observables in Lattice Field Theories with Deep Generative Models, *Phys. Rev. Lett.* 126 (2021) 032001. doi:10.1103/PhysRevLett.126.032001. [arXiv:2007.07115](#).
- [9] P. Białas, P. Korcyl, T. Stebel, Mutual information of spin systems from autoregressive neural networks, *Phys. Rev. E* 108 (2023) 044140. doi:10.1103/PhysRevE.108.044140. [arXiv:2304.13412](#).
- [10] P. Białas, P. Korcyl, T. Stebel, D. Zapolski, Rényi entanglement entropy of a spin chain with generative neural networks, *Phys. Rev. E* 110 (2024) 044116. doi:10.1103/PhysRevE.110.044116. [arXiv:2406.06193](#).
- [11] P. Białas, P. Korcyl, T. Stebel, Hierarchical autoregressive neural networks for statistical systems, *Comput. Phys. Commun.* 281 (2022) 108502. doi:10.1016/j.cpc.2022.108502. [arXiv:2203.10989](#).
- [12] P. C. J. M. Hammersley, Markov fields on finite graphs and lattices, 1971. URL: <http://www.statslab.cam.ac.uk/~grg/books/hammfest/hamm-cliff.pdf>.
- [13] P. Clifford, Markov random fields in statistics, in: *Disorder in Physical Systems. A Volume in Honour of John M. Hammersley*, Clarendon Press, 1990.
- [14] J. S. Liu, Metropolized independent sampling with comparisons to rejection sampling and importance sampling, *Statistics and Computing* 6 (1996) 113–119. URL: <https://doi.org/10.1007/BF00162521>. doi:10.1007/BF00162521.
- [15] A. Kong, A note on importance sampling using standardized weights, University of Chicago Technical Reports (1992).
- [16] A. van den Oord, N. Kalchbrenner, O. Vinyals, L. Espeholt, A. Graves, K. Kavukcuoglu, Conditional image generation with pixelcnn decoders (2016). doi:10.48550/arXiv.1606.05328. [arXiv:1606.05328](#).
- [17] A. Bulgarelli, M. Panero, Entanglement entropy from non-equilibrium Monte Carlo simulations, *JHEP* 06 (2023) 030. doi:10.1007/JHEP06(2023)030. [arXiv:2304.03311](#).